Theory of carrier depletion and light amplification in active slow light photonic crystal waveguides

Chen, Yaohui; Mørk, Jesper

Published in:
Optics Express

Link to article, DOI:
10.1364/OE.21.029392

Publication date:
2013

Document Version
Publisher's PDF, also known as Version of record

Theory of carrier depletion and light amplification in active slow light photonic crystal waveguides

Yaohui Chen* **and Jesper Mørk**

DTU Fotonik, Department of Photonics Engineering, Technical University of Denmark, Kgs. Lyngby, Denmark

*yach@fotonik.dtu.dk

Abstract: Using a perturbative approach, we perform a quantitative three-dimensional analysis of slow-light enhanced traveling wave amplification in an active semiconductor photonic crystal waveguide. The impact of slow-light propagation on the carrier-depletion-induced nonlinear gain saturation of the device is investigated. An effective rate-equation-based model is presented. It is shown that it well accounts for the three-dimensional simulation results. Simulations indicate that a slow-light-enhanced photonic crystal traveling-wave amplifier has a high small-signal modal gain and low saturation power.

OCIS codes: (250.5980) Semiconductor optical amplifiers; (130.5296) Photonic crystal waveguides.

References and links

1. T. Baba, "Slow light in photonic crystals," Nat. Photonics **2**, 465–473 (2008).
2. J. P. Dowling, M. Scalora, M. J. Bloemer, and C. M. Bowden, "The photonic band edge laser: A new approach to gain enhancement," J. Appl. Phys. **75**, 1896–1899 (1994).
3. J. Mørk and T. R. Nielsen, "On the use of slow light for enhancing waveguide properties," Opt. Lett. **35**, 2834–2836 (2010).
4. E. Mizuta, H. Watanabe, and T. Baba, "All semiconductor low-Δ photonic crystal waveguide for semiconductor optical amplifier," Jpn. J. Appl. Phys. **45**, 6116–6120 (2006).
5. R. Kappeler, P. Kasper, H. Jäckel, and C. Hafner, "Record-low propagation losses of 154dB/cm for substrate-type W1 photonic crystal waveguides by means of hole shape engineering," Appl. Phys. Lett. **101**, 131108 (2012).
6. S. Matsuo, A. Shinya, T. Kakitsuka, K. Nozaki, T. Segawa, T. Sato, Y. Kawaguchi, and M. Notomi, "High-speed ultracompact buried heterostructure photonic-crystal laser with 13fJ of energy consumed per bit transmitted," Nat. Photonics **4**, 648–654 (2010).
7. B. Ellis, M. A. Mayer, G. Shambat, T. Sarmiento, J. Harris, E. E. Haller, and J. Vuckovic, "Ultralow-threshold electrically pumped quantum-dot photonic-crystal nanocavity laser," Nat. Photonics **5**, 297–300 (2011).
8. K. Takeda, T. Sato, A. Shinya, K. Nozaki, W. Kobayashi, H. Taniyama, M. Notomi, K. Hasebe, T. Kakitsuka, and S. Matsuo, "Few-fJ/bit data transmission using directly modulated lambda-scale embedded active region photonic-crystal lasers," Nat. Photonics **7**, 569–575 (2013).
9. P. Bermel, E. Lidorikis, Y. Fink, and J. D. Joannopoulos, "Active materials embedded in photonic crystals and coupled to electromagnetic radiation," Phys. Rev. B **73**, 165125 (2006).
10. Y. Liu, "Slow-light enhancement of stimulated emission of atomic systems in photonic crystals," J. Opt. Soc. Am. B **27** 442–446 (2010).
11. A. Mock, "First principles derivation of microcavity semiconductor laser threshold condition and its application to FDTD active cavity modeling," J. Opt. Soc. Am. B **27**, 2262–2272 (2010).
12. L. A. Coldren and S. W. Corzine, *Diode Lasers and Photonic Integrated Circuits* (John Wiley, 1995).
13. G. P. Agrawal and N. A. Olsson, "Self-phase modulation and spectral broadening of optical pulses in semiconductor laser amplifiers," IEEE J. Quantum Electron. **25**, 2297–2306 (1989).

#197786 - $15.00 USD Received 16 Sep 2013; revised 13 Nov 2013; accepted 13 Nov 2013; published 21 Nov 2013

14. P. Borri, S. Scaffetti, J. Mørk, W. Langbein, J. M. Hvam, A. Mecozzi, and F. Martelli, "Measurement and calculation of the critical pulsewidth for gain saturation in semiconductor optical amplifiers," Opt. Commun. **164**, 51–55 (1999).
15. J. Mørk, A. Mecozzi, and G. Eisenstein, "The modulation response of a semiconductor laser amplifier," IEEE J. Sel. Top. Quantum Electron. **5**, 851–860 (1999).
16. B. Tromborg, H. E. Lassen, and H. Olesen, "Traveling wave analysis of semiconductor lasers: Modulation responses, mode stability and quantum mechanical treatment of noise spectra," IEEE J. Quantum Electron. **30**, 939–956 (1994).
17. www.comsol.com.
18. J. E. Sipe, N. A. R. Bhat, P. Chak, and S. Pereira, "Effective field theory for the nonlinear optical properties of photonic crystal," Phys. Rev. E **69,** 016604 (2004).
19. N. C. Panoiu, J. F. MicMillan, and C. W. Wong, "Theoretical analysis of pulse dynamics in silicon photonic crystal wire waveguides," IEEE J. Sel. Top. Quantum Electron. **16**, 257–266 (2010).
20. A. Mecozzi and J. Mørk, "Theory of heterodyne pump-probe experiments with femtosecond pulses," J. Opt. Soc. Am. B **13**, 2437–2452 (1996).
21. S. G. Johnson and J. D. Joannopoulos, "Bloch-iterative frequency-domain methods for Maxwell's equations in a planewave basis," Opt. Express **8**, 173–190 (2001).
22. A. Taflove, *Computational Electrodynamics: The Finite-Difference Time-Domain Method* (Artech House, 1995).
23. J. S. Jensen and O. Sigmund, "Topology optimization for nano-photonics," Laser Photonics Rev. **5**, 308–321 (2011).
24. A. F. Oskooi, D. Roundy, M. Ibanescu, P. Bermel, J. D. Joannopoulos, and S. G. Johnson, "Meep: A flexible free-software package for electromagnetic simulations by the FDTD method," Comput. Phys. Commun. **181**, 687–702 (2010).
25. K. Schmidt and R. Kappeler, "Efficient computation of photonic crystal waveguide modes with dispersive material," Opt. Express **18**, 7307–7322 (2010).
26. C. Fietz, Y. Urzhumov, and G. Shvets, "Complex k band diagrams of 3D metamaterial/photonic crystals," Opt. Express **19**, 19027–19041 (2011).
27. T. Tanabe, H. Taniyama, and M. Notomi, "Carrier diffusion and recombination in photonic crystal nanocavity optical switches," J. Lightwave Technol. **26**, 1396–1403 (2008).
28. J. Petykiewicz, G. Shambat, B. Ellis, and J. Vuckovic, "Electrical properties of GaAs photonic crystal cavity lateral p-i-n diodes," Appl. Phys. Lett. **101**, 011104 (2012).
29. T. Lund-Hansen, S. Stobbe, B. Julsgaard, H. Thyrrestrup, T. Sünner, M. Kamp, A. Forchel, and P. Lodahl, "Experimental realization of highly-efficient broadband coupling of single quantum dots to a photonic crystal waveguide," Phys. Rev. Lett. **101**, 113903 (2008).
30. T. Liu, K. Obermann, K. Petermann, F. Girardin, and G. Guekos, "Effect of saturation caused by amplified spontaneous emission on semiconductor optical amplifier performance," Electron. Lett. **33**, 2042–2043 (1997).
31. L. O' Faolain, S. A. Schulz, D. M. Beggs, T. P. White, M. Spasenovic, L. Kuipers, F. Morichetti, A. Melloni, S. Mazoyer, J. P. Hugonin, P. Lalanne, and T. F. Krauss, "Loss engineered slow light waveguides," Opt. Express **18**, 27627–27638 (2010).
32. J. Grgic, J. R. Ott, F. Wang, O. Sigmund, A. P. Jauho, J. Mørk, and N. A. Mortensen, "Fundamental limitations to gain enhancement in periodic media and waveguides," Phys. Rev. Lett. **108**, 183903 (2012).
33. F. A. Kish, D. Welch, R. Nagarajan, J. L. Pleumeekers, V. Lal, M. Ziari, A. Nilsson, M. Kato, S. Murthy, P. Evans, S. W. Corzine, M. Mitchell, P. Samra, M. Missey, S. DeMars, R. P. Schneider, M. S. Reffle, T. Butrie, J. T. Rahn, M. Van Leeuwen, J. W. Stewart, D. J. H. Lambert, R. C. Muthiah, H.-S. Tsai, J. S. Bostak, A. Dentai, K.-T. Wu, H. Sun, D. J. Pavinski, J. Zhang, J. Tang, J. McNicol, M. Kuntz, V. Dominic, B. D. Taylor, R. A. Salvatore, M. Fisher, A. Spannagel, E. Strzelecka, P. Studenkov, M. Raburn, W. Williams, D. Christini, K. K. Thomson, S. S. Agashe, R. Malendevich, G. Goldfarb, S. Melle, C. Joyner, M. Kaufman, and S. G. Grubb, "Current status of large-scale inp photonic integrated circuits," IEEE J. Sel. Top. Quantum Electron. **17**, 1470–1489 (2011).
34. J. Mørk, P. Lunnemann, W. Xue, Y. Chen, P. Kaer, and T. R. Nielsen, "Slow and fast light in semiconductor waveguides," Semicond. Sci. Technol. **25**, 083002 (2010).
35. M. L. Nielsen and J. Mørk, "Increasing the modulation bandwidth of semiconductor-optical-amplifier-based switches by using optical filtering," J. Opt. Soc. Am. B **21**, 1606–1619, (2004).

1. Introduction

Photonic crystal (PhC) structures have been proposed as a waveguide infrastructure for high-density photonic integrated circuits (PICs). Optical amplification is one of the fundamental functionalities, required for compensating attenuation and coupling losses and thus increasing the number of integrated devices. A major advantage in combining PhC waveguides and active III-V semiconductors is the possibility to drastically decrease the component length via

#197786 - $15.00 USD Received 16 Sep 2013; revised 13 Nov 2013; accepted 13 Nov 2013; published 21 Nov 2013

enhanced light-matter interaction enabled by slow-light (SL) propagation [1]. The investigation of group velocity related gain enhancement was initiated in Bragg slabs [2]. It is natural to extend such idea to PhC line defect waveguides with guided modes within the bandgap [3]. Attempts of realizing PhC travelling wave semiconductor optical amplifiers (SOAs) [4] are confronted by various challenges, e.g. excessive propagation losses due to mode leakage into substrate [5] as well as heating issues. However, recent progress within PhC Lasers [6, 7, 8] witness the continued development of the PhC membrane platform, indicating the feasibility of realizing PhC amplifiers.

In order to simulate the properties of PhC SOAs, one needs simultaneously to account for the electromagnetic field distribution and propagation in the membrane as well as its coupling to the carriers in the active region of the structure, typically layers of quantum wells or quantum dots. The strong dispersion originating from the PhC structuring makes this coupling highly non-trivial. The finite difference time domain (FDTD) method has been used to simulate the properties of an active material, often described by Maxwell-Bloch equations, embedded in different types of PhC structures[9, 10, 11]. Because gain saturation can be only properly evaluated when the time-domain simulation reaches steady state, this time-domain approach is computationally demanding and not suitable for systematic investigations in practice.

Thus what is missing is an effective model equivalent to the traveling wave model of an active ridge waveguide [12], which has been so successful in understanding the properties of SOAs as well as lasers, e.g., gain saturation [13, 14], small-signal modulation response [15] and laser dynamics [12, 16]. A one-dimensional rate equation analysis [4] with heuristic inclusion of group velocity was used to investigate the gain characteristics of PhC traveling wave SOAs, but was not validated against full simulations. We note that while the group index does show up in the standard formulation of the traveling wave equation for conventional SOAs, the replacement of that group index with a value enhanced by the slow-down factor due to PhC induced dispersion has to be justified. Such an approach ignores that the implicit quasi-plane wave approximation used in classical ridge waveguide amplifier and laser models is no longer appropriate for structured optical waveguides with strong dispersion.

In this paper we present a theoretical analysis that quantifies the carrier depletion and continuous-wave (CW) light amplification in active PhC waveguides based on a perturbative approach. Taking advantage of the perturbative treatment, we decouple the two physical subsystems and conduct extensive finite-element (FE) simulations [17] for time-harmonic vectorial fields in the reference passive PhC membrane waveguide, while separately accounting for the corresponding microscopic carrier depletion within the embedded gain region. Moreover, we suggest a modified rate equation model that well accounts for the carrier-depletion-induced modal gain saturation in a SL-enhanced active PhC waveguide.

2. Theory

In the weak perturbation limit [18, 19] for CW light amplification, the electric and magnetic fields of the principal guided Bloch wave, $[\mathbf{E}(r,t),\mathbf{H}(r,t)]$, of an active PhC waveguide at a given frequency ω are approximated as:

$$[\mathbf{E}(r,t),\mathbf{H}(r,t)] = \frac{1}{2}[\mathbf{e}(r),\mathbf{h}(r)]\psi(z)\exp(i\beta z - i\omega t) + c.c., \tag{1}$$

Here β is the wave number along the propagation direction z, $\psi(z)$ is the amplitude of the forward propagating field component, $\mathbf{e}(r),\mathbf{h}(r)$ are the normalized electric and magnetic fields of the periodic Bloch mode in passive structure.

The carrier-induced polarization $\mathbf{P}_{pert}(r,t)$ in the gain medium is approximated as:

$$\mathbf{P}_{pert}(r,t) = \frac{1}{2}\varepsilon_0\chi_{pert}(r)\mathbf{e}(r)\psi(z)\exp(i\beta z - i\omega t) + c.c., \tag{2}$$

#197786 - $15.00 USD Received 16 Sep 2013; revised 13 Nov 2013; accepted 13 Nov 2013; published 21 Nov 2013

where ε_0 is electric permittivity of free space and $\chi_{pert}(r)$ is the first-order susceptibility change, which is determined by the carrier-induced material gain, $g(r) = g_{mat}F(r)f_{inv}(r)$, as the product of maximum material gain, g_{mat}, active material distribution function, $F(r)$ and distributed population inversion factor, $f_{inv}(r)$. For simplicity, material dispersion is not taken into account.

In equilibrium, we have the following balance condition involving the carrier density $N(r)$:

$$0 \quad = \quad R_p(r) - R_{st}(r) - \frac{N(r)}{\tau_s}, \tag{3}$$

where τ_s is carrier lifetime, $R_p(r)$ is the distributed injection rate of carriers by optical/electrical pumping, $R_{st}(r)$ is the local stimulated emission rate which generally depends on the carrier-induced polarization change:

$$R_{st}(r) \quad = \quad \frac{\mathrm{Im}\{\omega \mathbf{P}^*_{pert}(r) \cdot \mathbf{E}(r)\}}{\hbar\omega} \tag{4}$$

By substituting Eq. (1) and Eq. (2) into Eq. (4), the stimulated emission rate becomes:

$$R_{st}(r) \quad = \quad \frac{1}{\hbar\omega}\frac{c}{n_b} g_{mat}F(r)f_{inv}(r) \cdot \frac{2}{4}\varepsilon_0 n_b^2 |\mathbf{e}(r)|^2 |\psi(z)|^2 \tag{5}$$

$$= \quad \frac{\Gamma g_{mat} a}{\hbar\omega}\frac{n_g}{n_b}\frac{\varepsilon_0 n_b^2 F(r)|\mathbf{e}(r)|^2 f_{inv}(r)}{\langle \varepsilon_0 n_b^2 F(r)|\mathbf{e}(r)|^2\rangle} |\psi(z)|^2 P_z, \qquad \Gamma \equiv \frac{\langle \varepsilon_0 n_b^2 F(r)|\mathbf{e}(r)|^2\rangle}{\langle \varepsilon_0 n_b^2(r)|\mathbf{e}(r)|^2\rangle} \tag{6}$$

Here c is the speed of light in vacuum, n_g is the group index along propagation direction z, accounting for the propagation speed governed by the PhC waveguide dispersion, n_b is the background refractive index, $\hbar$ is Plank's constant. Volume integration operator over a supercell is indicated by $\langle\rangle$. Furthermore, a is the lattice constant, $P_z = \frac{1}{2}\int_s \mathrm{Re}\{\mathbf{e}(r) \times \mathbf{h}^*(r)\} \cdot \hat{\mathbf{z}} dS$ is the unit rms power flux over the transverse section, which is related to unit rms electric and magnetic energy stored in a supercell $\langle W\rangle = a n_g P_z/c$ and Γ is the confinement factor giving the fraction of electric energy stored inside the active region. Here $f_{inv}(r)$ and $N(r)$ in the active material are implicitly determined by a Fermi-Dirac integral under quasi-equilibrium condition.

Within the slowly-varying envelope assumption, $\psi(z)$ is considered constant over the period, a, of the PhC structure. The modal gain per unit length based on Poynting's theorem is quantified as:

$$g_{mod} = \frac{\hbar\omega\langle R_{st}(r)\rangle}{a|\psi(0)|^2 P_z} = \Gamma g_{mat}\frac{n_g}{n_b}\bar{f}_{inv}, \qquad \bar{f}_{inv} = \frac{\langle \varepsilon_0 n_b^2 F(r)|\mathbf{e}(r)|^2 f_{inv}(r)\rangle}{\langle \varepsilon_0 n_b^2 F(r)|\mathbf{e}(r)|^2\rangle} \tag{7}$$

With $\bar{f}_{inv}$ being a volume-averaged population inversion factor.

Our modal gain approximation for active PhC waveguides is consistent with the perturbative analysis based on quasi-planar wave expansion in conventional active semiconductor waveguides by separating transverse mode distribution and longitudinal field envelope [12]. Thus Eq. (7) reduces to the well-known expression for the modal gain per unit length for conventional ridge waveguide structures. The difference is that in the conventional quasi-planar ridge waveguide the group index induced by waveguide dispersion is fairly close to the background refractive index and there is little room for dispersion engineering. Hence, we consider Eq. (7) reduces to the well-known modal gain (per unit length) definition primarily determined by optical mode confinement factor over the transverse cross section.

3. Effective rate equation analysis

Alternatively, we suggest a modified effective rate equation analysis. Based on Eq. (3) and energy conservation, we derive a balance equation for the averaged carrier density $\langle N\rangle/V_{act}$ in

#197786 - $15.00 USD Received 16 Sep 2013; revised 13 Nov 2013; accepted 13 Nov 2013; published 21 Nov 2013

a supercell:

$$0 = \frac{\langle R_P \rangle}{V_{act}} - \frac{\langle R_{st} \rangle}{V_{act}} - \frac{\langle N \rangle}{V_{act}\tau_s}, \tag{8}$$

$$\frac{\langle R_{st} \rangle}{V_{act}} = \frac{g_{mat}}{\hbar\omega}\frac{\Gamma a}{V_{act}}\frac{n_g}{n_b}\bar{f}_{inv}|\psi(z)|^2 P_z = g_{mat}\frac{c}{n_b}\frac{\Gamma V_{opt}}{V_{act}}\bar{f}_{inv}|\psi(z)|^2 N_P \tag{9}$$

Here V_{act} and V_{opt} are the active material and optical mode volume. We define the optical mode volume V_{opt} in passive PhC waveguides as:

$$V_{opt} = \frac{\langle \varepsilon_0 n_b(r)^2 |\mathbf{e}(r)|^2 \rangle}{0.5\{\varepsilon_0 n_b(r)^2 |\mathbf{e}(r)|^2\}_{max}} \tag{10}$$

Here, volume integration operator over a supercell is indicated by $\langle\rangle$ and the averaged electrical energy density is defined as half of the maximum density value. $N_p = n_g a P_z/(\hbar\omega V_{opt} c)$ is the averaged photon density corresponding to the unit rms power flux P_z. Eq. (8) with scalar field approximation in quasi-planar waveguides is equivalent to the stationary form of conventional laser dynamics rate equation analysis [12]. The equivalent effective area defined in conventional SOAs is $A_{eff} = V_{opt}/a$.

For simplicity, we may approximate the active material volume as $V_{act} = \Gamma V_{opt}$. The confinement factor in the stimulated emission term as a function of photon density [4] is justified by $\Gamma V_{opt}/V_{act}$. The ratio V_{opt}/V_{act} reminds us that the investigated averaged carrier and photon densities are quantities normalized by difference volume definitions. By assuming that carrier and photon densities are uniformly distributed inside the corresponding volumes, both V_{act} and V_{opt} are extra free parameters in this effective model. In particular, V_{act} is phenomenologically introduced to describe the active material region, where carriers interact with light. We notice that, as in conventional SOAs [20], the relevant definition of the confinement factor depends on how the considered saturation mechanism scales with the field intensities. For carrier dynamical contributions with various physical origins, additional correction factors for V_{act} are required to allow this effective model to provide reasonable approximation of microscopic simulation results.

4. Simulation results and discussions

We consider a W1 line-defect PhC membrane with quantum well (QW) layers embedded in the middle of the membrane, as shown in Fig. 1. The parameters are chosen to realize single mode traveling-wave optical amplification in the C-band for an InGaAsP membrane. To model the quantum well, we use a simple free carrier gain model with homogeneous carrier pumping over the extent of the PhC membrane.

Our numerical simulations start by solving for the time-harmonic guided mode in the passive three-dimensional PhC waveguide, which is an eigenmode problem governed by Maxwell's equations with Bloch theorem. Many popular numerical methods and codes, e.g., MIT Photonic Bands (MPB) based on plane wave expansion in a supercell [21], FDTD eigenmode extraction based on a proper pulsed excitation in a periodic system [22] and finite-element (FE) analysis of a superccell [23], are available to evaluate such eigenvalue problem with different computational cost and efficiency [24, 25]. In this paper, we implement FE vectorial field eigenmode calculations [26] of three-dimensional passive W1 line-defect PhC membrane waveguide based on a supercell approach. Examples of time-averaged electric energy density profiles of a typical fundamental TE-like guided mode at the wavelength of 1550nm are shown in Fig. 1(b). The relevant guided modes in the PhC membrane waveguide are tightly confined horizontally by the band gap and vertically by index guiding.

#197786 - $15.00 USD Received 16 Sep 2013; revised 13 Nov 2013; accepted 13 Nov 2013; published 21 Nov 2013

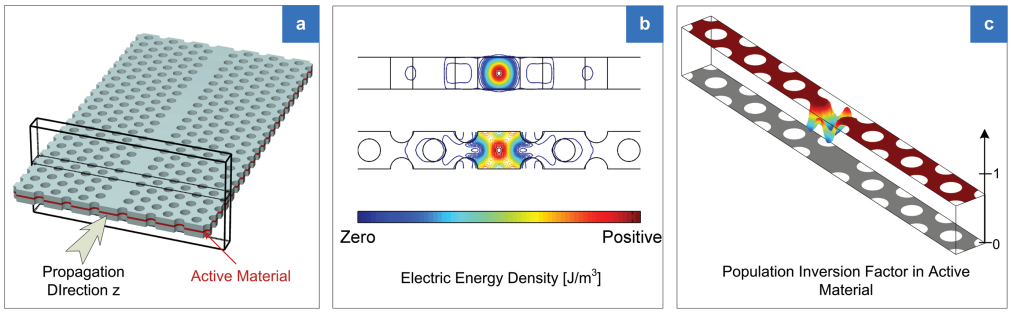

Fig. 1. (a) Schematic of active photonic crystal membrane waveguide with a single quantum well layer embedded in the middle of the membrane. (b) Optical mode profile of fundamental TE-like guided modes at $\lambda = 1550$nm in the reference passive W1 line-defect photonic crystal membrane waveguide: Side- and top-views of time-averaged electric energy density. (c) Depleted population inversion factor in active material. (Parameters: lattice period a=398nm, air-hole radius r=0.3a, membrane thickness h=0.85a, background refractive index $n_b = \sqrt{11.2}$, quantum well thickness h_{QW}=10nm).

Based on the knowledge of the calculated Bloch mode profiles, we proceed to analyze the microscopic carrier density distribution in the active material based on Eq. (3). For a given input optical power, the high concentration of electric field intensity in the line-defect region leads to the corresponding non-uniformly depleted carrier density (population inversion factor) distribution as shown in Fig. 1(c). The strength of our theoretical analysis is to approximate and decouple the two physical subsystems within the perturbative limit, thus avoiding repeated eigenmode calculations when only considering small deviations from the passive mode. Such approach allows us to conduct comprehensive parameter sweeps. In order to highlight the slow-light impact on stimulated emission, we neglected the details of carrier diffusion and surface-recombination and just consider the carrier dynamics to be governed by a single decay time. This is similar to the case of conventional SOAs and the analysis can easily be expanded to include more elaborated carrier transport phenomena in semiconductor devices governed by Poisson and carrier drift-diffusion equations under realistic assumptions [27, 28]. Furthermore, the slow-light impact on spontaneous emission may be explicitly included into Eq. (3) as modified radiative recombinations contributing to the carrier lifetime [29]. The saturation caused by amplified spontaneous emission [30] can be further investigated to determine the condition for optimum performance.

Figure 2 illustrates the calculated band diagram and frequency dependence of the parameters entering Eq. (6) for SL-enhanced modal gain in a 3D PhC waveguide with a single QW layer. In the small-signal limit, $f_{inv}(r)$, which is derived from the Fermi-Dirac distribution, is constant within the active region under uniform pumping. Due to different loss mechanisms [31] in practical SL PhC waveguides and fundamental limitations to gain enhancement close to the photonic bandedge [32], we limit our discussion to slow light modes with group index up to around 40 and relatively small maximum material gain $g_{mat} = 1000cm^{-1}$. For the given carrier-induced susceptibility and active material filling factor, the perturbative expression for the modal gain has excellent agreement with the imaginary part of the wavenumber obtained from (numerically exact) FEM simulations of active waveguides. The relative error of the modal gain is on the order of 0.1% or less. As the frequency decreases towards the band-edge region, the enhancement of the modal gain is dominated by the increased group index. Meanwhile, the corresponding optical mode volume for averaged electric energy density gradually increases as the optical fields extend into the cladding photonic crystal region, which will also impact on the

#197786 - $15.00 USD Received 16 Sep 2013; revised 13 Nov 2013; accepted 13 Nov 2013; published 21 Nov 2013

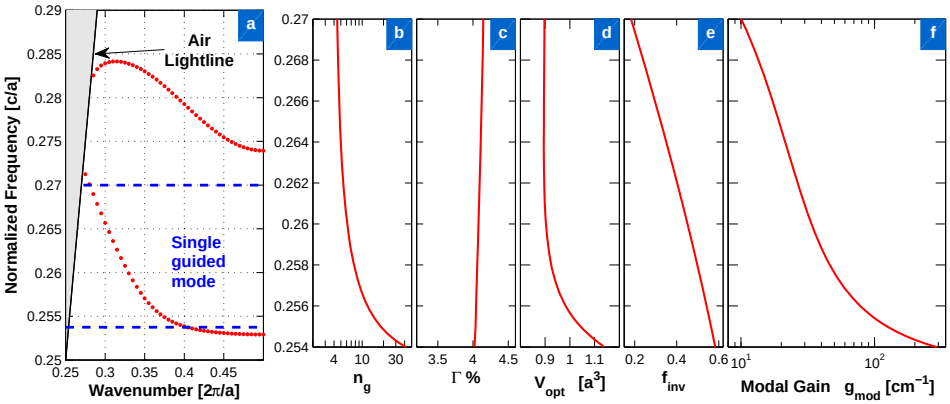

Fig. 2. Calculated slow-light enhanced small-signal modal gain in a W1 line-defect PhC membrane with a single QW layer. (a) Band diagram of passive PhC waveguide. (b) Group index n_g; (c) confinement factor $\Gamma\%$; (d) optical mode volume for averaged electric energy density V_{opt}; (e) population inversion factor f_{inv}; (f) modal gain g_{mod} as a function of normalized frequency. ($g_{mat} = 1000cm^{-1}$).

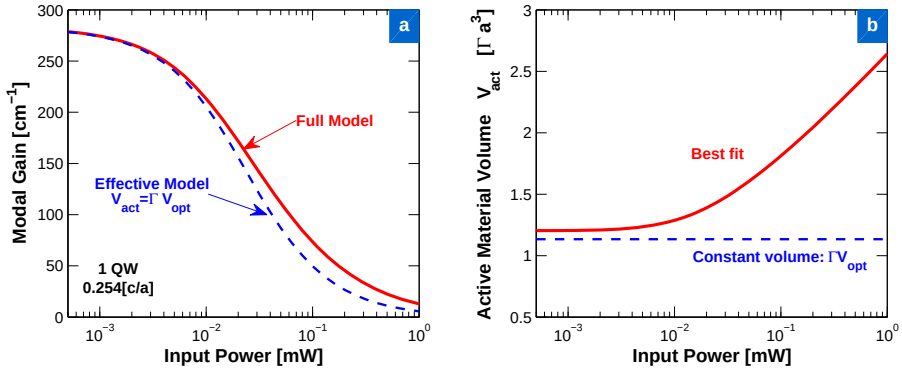

Fig. 3. Slow-light-enhanced modal gain saturation in a W1 line-defect PhC membrane with a single QW layer. (a) Comparison of modal gain as a function of input power between: full model with microscopic carrier depletion description, Eq. (3), and effective model with averaged carrier depletion description, Eq. (8), with constant active material volume $V_{act} = \Gamma V_{opt}$. (b) Best fit of active material volume V_{act}, to be used in the effective model, as a function of input power in effective model. Dashed line gives the value of ΓV_{opt}. Normalized frequency 0.254[c/a].

averaged photon density for the effective model, Eq. (8) and the gain saturation profile.

Figure 3 illustrates the SL-enhanced modal gain saturation in PhC waveguides. Figure 3(a) shows that the effective model using a constant value of the active material volume $V_{act} = \Gamma V_{opt}$ agrees well with the full model results with microscopic carrier depletion description based on Eq. (3). In order to achieve better agreement between the effective model and the full model, we may allow the effective volume to vary as a function of power as shown in Fig. 3(b). The best fit active volume is seen to increase and deviate from the constant volume ΓV_{opt} for large input power levels. In this case, we are investigating an active PhC waveguide, in which the active QW layers have the same lateral extent as that of PhC waveguides. A large input power

#197786 - $15.00 USD Received 16 Sep 2013; revised 13 Nov 2013; accepted 13 Nov 2013; published 21 Nov 2013

level leads to the non-uniformly depleted carrier density, in particular, around the peak energy density spot in the middle of the line-defect region. However, the tail of the optical fields can still experience significant gain in the less depleted cladding photonic crystal region. Hence, the effective active volume increases with the rising of input power levels.

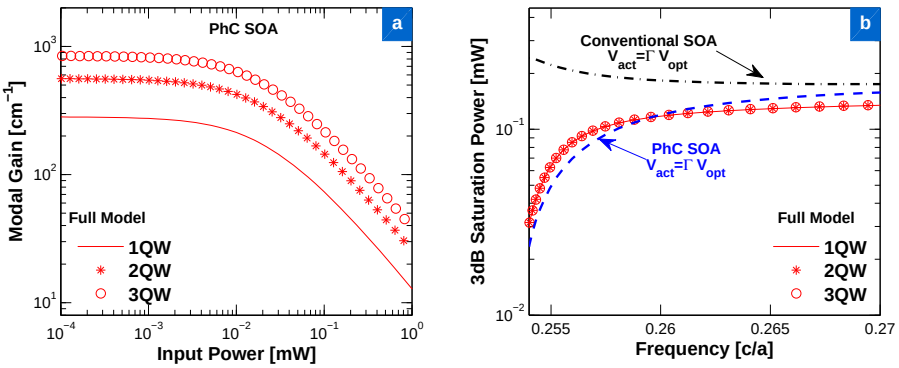

Fig. 4. Slow-light-enhanced modal gain saturation in a W1 line-defect PhC membrane with different number of QW layers based on full model. (a) Modal gain as a function of input power. Normalized frequency 0.254[c/a]. (b) 3dB saturation power as a function of frequency. Dashed line indicates the 3dB saturation power of PhC waveguide based on effective model with $V_{act} = \Gamma V_{opt}$. Dash dotted line indicates the results for a conventional SOA based on effective model with a constant group index $n_g = 4$ and other parameters assumed identical to the PhC waveguides.

Figure 4(a) illustrates the gain saturation in PhC waveguides with different QW layer numbers. By increasing the number of QW layers, the confinement factor is increased proportionally. Hence, larger modal gain is provided for traveling wave amplification. On the other hand, the corresponding 3dB saturation power shown in Fig. 4(b) has negligible dependence on the number of QW layers. As V_{act} is also proportional to the number of QW layers, the factors $\Gamma a/V_{opt}$ and $\Gamma V_{opt}/V_{act}$ are hardly changed. As the operation frequency moves deeper into the slow-light region, the saturation power further decreases. For the frequency range of interest, the saturation powers are well approximated by the effective model with constant active material volume $V_{act} = \Gamma V_{opt}$. In contrast, the saturation power in conventional SOAs is rather insensitive to operation frequency since both group index and confinement factor in standard ridge waveguide designs have small variations against frequency. The dash dotted line in Fig. 4(b) shows the saturation power for a conventional SOA with a group index of 4 and other parameters (i.e. confinement and optical mode volume) assumed identical to those of the PhC waveguides. The slight increase of saturation power for lower optical frequency reflects that more carriers are available for stimulated emissions close to the band edge. The ratio of the saturation power at normalized frequency 0.254[c/a] corresponds to the ratio between the group indices of the two waveguides. In practice, the conventional SOAs have larger effective area A_{eff}, on the order of $1\mu m^2$, which leads to further increase of saturation power level.

Such strongly frequency-dependent modal gain and 3dB-saturation power make the device less attractive for broadband linear amplification, e.g., in PICs employing wavelength-division multiplexing [33], while the flexibility in controlling the gain dispersion and the significantly decreased saturation power in the SL region may be attractive for many SOA-based nonlinear optical signal processing applications, e.g. microwave phase shifters based on four-wave mixing (FWM) and coherent population oscillation (CPO) effects [34], optical switching utilizing cross gain modulation (XGM) and cross phase modulation (XPM) effects [35] .

#197786 - $15.00 USD Received 16 Sep 2013; revised 13 Nov 2013; accepted 13 Nov 2013; published 21 Nov 2013

5. Summary

We compared rigorous three-dimensional simulations of gain saturation in photonic crystal active waveguides to the predictions of an effective rate-equation-based model. The simple rate equation model well accounts for the carrier-depletion-induced modal gain saturation in active semiconductor waveguides. Simulations indicate that a slow-light-enhanced photonic crystal traveling-wave amplifier has a high small-signal modal gain and low saturation power, making it promising for nonlinear optical signal processing.

Acknowledgments

The authors acknowledge support from the NATEC centre funded by VILLUM FONDEN and the Danish Council for Independent Research (Grant No.: 10-081396).

#197786 - $15.00 USD Received 16 Sep 2013; revised 13 Nov 2013; accepted 13 Nov 2013; published 21 Nov 2013